J Mater Sci (2007) 42:2244–2249
DOI 10.1007/s10853-006-0077-9

Nonhydrolytic sol-gel synthesis and characterization of YAG

Eduardo José Nassar · Paula Fabiana dos Santos Pereira · Evelisy Cristina de Oliveira Nassor · Lilian Rodrigues Ávila · Katia Jorge Ciuffi · Paulo Sergio Calefi

Received: 1 November 2005 / Accepted: 27 March 2006 / Published online: 23 January 2007

Abstract Yttrium–aluminum oxides are interesting compounds, which are widely used as hosts for lasers and phosphors due to their stable physical and chemical properties. The manufacture of YAG has been investigated thoroughly. YAG powders are traditionally synthesized through the reaction of aluminum and yttrium powders at high temperatures. The work reported here involved an investigation into the preparation of YAG by a nonhydrolytic sol-gel route and the influence of heating time at low temperatures to obtain YAG from inorganic precursors (yttrium and aluminum chloride). $AlCl_3$, YCl_3 and ethanol were reflux reacted under an argon atmosphere. Europium III chloride was added as a structural probe. The powder was treated at 800 °C for 1, 2, 4, 8 and 16 h. The YAG structure was analyzed by X-ray diffraction (XRD), nuclear magnetic resonance (NMR), thermal analysis (TA) and photoluminescence (PL). The XRD revealed only peaks corresponding to the YAG phase. PL data showed that the YAG phase was formed in 2 min with samples pretreated at 50 °C. For the samples pretreated at 800 °C, the YAG phase appeared in 30 s. The excitation spectra presented a maximum of 394 nm corresponding to the $^5L_6$ level, while the emission spectra of Eu III ions showed characteristic transition bands arising from the $^5D_0 \rightarrow {}^7F_J$ (J = 1, 2, 3, 4) manifolds at maximum excitation. The magnetic dipole $^5D_0 \rightarrow {}^7F_1$ transition exhibited greater intensity than the electric dipole $^5D_0 \rightarrow {}^7F_2$ transition. This methodology proved efficient for obtaining YAG phase.

E. J. Nassar (✉) · P. F. dos Santos Pereira · E. C. de Oliveira Nassor · L. R. Ávila · K. J. Ciuffi · P. S. Calefi
Universidade de Franca, Av.Dr.Armando Salles Oliveira, 201, Franca, SP 14404-600, Brazil
e-mail: ejnassar@unifran.br

Introduction

The yttria–alumina system comprises three crystalline phases: $Y_3Al_5O_{12}$, $Y_4Al_2O_9$ and $YAlO_3$ [1]. YAG (yttrium–aluminum garnet) garnet phases, which are excellent materials with stable physical and chemical properties, are widely applied as hosts for lasers and phosphors due to the interesting optical properties of their cubic garnet structure [1–4]. YAG is of great interest as a high temperature engineering material thanks to its high temperature strength coupled with low creep rates [5]. Single crystals of Ce^{3+} doped YAG are applied in solid-state lasers. Ce^{3+} activated YAG powder is a fast-response flying-spot scanner phosphor, and Tb^{3+} doped YAG gives a narrow-bond phosphor characteristic suitable for contrast-enhanced display applications [4]. Er^{3+} doped YAG lasers are attractive and have become affordable for clinical use in dental tissue removal by ablative processes thanks to recent developments in diode laser and solid-state laser technology [6]. Nd^{3+}:YAG is a well known laser material thanks to its high optical quality, which is characteristic of single-crystal ceramics with potential application for the near infrared laser system [7, 8].

YAG is normally synthesized at high temperatures by solid-state reaction between aluminum and yttrium oxide. However, such processing conditions lead to several problems such as inappropriate particle sizes,

impurities, formation of undesirable phases, etc. [9]. Although the sol-gel route has been known for many years, it only began to be widely employed in the last few decades, mainly based on alkoxide. This process involves the preparation of colloidal suspensions, which are then transformed into viscous gels and solid materials [10]. The traditional sol-gel process offers various advantages, including low temperature entrapment of organic species, but its limitations, particularly the sensitive moisture precursors it requires, may negatively affect the end materials [1, 9]. To overcome these limitations, the nonhydrolytic sol-gel process—a versatile method of producing inorganic oxides and mixed oxides—was developed as an alternative methodology [11]. The nonhydrolytic sol-gel route involves the reaction of a metal halide with an oxygen donor such as an ether, alcohol or other donor under nonaqueous conditions to form an inorganic oxide [12].

In this work we investigate the influence of the heat treatment time in the preparation of YAG by a nonhydrolytic sol-gel route. Eu^{3+} doped with aluminum–yttrium oxide was synthesized by a nonhydrolytic sol-gel method using yttrium and aluminum chloride [13]. The powder thus obtained was dried and treated at 800 °C for 1, 2, 4, 8 and 16 h.

The formation process and structure of the powder were analyzed by X-ray Diffraction (XRD), Thermal Analysis (TG/DTA), Photoluminescence (PL) and Nuclear Magnetic Resonance of ^{27}Al (NMR).

Experimental

Europium and yttrium chloride (1×10^{-1} mol/L) were prepared from their oxides (Aldrich). Eu_2O_3 and Y_2O_3 were dissolved with HCl in deionized water, followed by evaporation to remove the acid. Rare earth salts ($TRCl_3$) were dissolved with anhydrous ethanol.

The gel was prepared in oven-dried glassware. The material was synthesized using a modified version of the method described by Acosta et al. [14]. One gram of aluminum chloride ($AlCl_3$) and 25 mL of ethanol (EtOH), used as the only oxygen donor, was reacted with yttrium chloride in a molar ratio of 5:3, adding 1.0% of $EuCl_3$ as structural probe. The mixture remained in reflux for 4 h at 110 °C in 50 mL of dry DCM (previously distilled) in an argon atmosphere. A condenser was placed in a thermostatic bath at –5 °C. The gel was formed after 90 min of reaction and a solid material began to precipitate after 30 min. After reflux, the mixture was cooled and aged overnight in the mother liquor at room temperature. The solvent was then removed under vacuum. The powder was dried and heat-treated at 800 °C for 1, 2, 4, 8 and 16 h.

The XRD measurements were taken at room temperature with a Rigaku Geigerflex D/max-c diffractometer using monochromated CuK_α radiation ($\lambda = 1.54$ Å) in the 2θ range from 4 to 80° at a resolution of 0.05°.

Thermal analysis (TG/DTA) was carried out (Thermal Analyst 2100—TA Instruments SDT 2960 simultaneous DTA-TG) in a nitrogen atmosphere at a heating rate of 20 °C min^{-1}, from 25 to 1,500 °C.

An ^{27}Al NMR (59.5 MHz) analysis was done with an INOVA 300 Varian spectrophotometer, using silicon nitride as reference.

Photoluminescence data were obtained under continuous Xe lamp (450 W) excitation with a spectrofluometer (SPEX-Fluorolog II) at room temperature. The emission was collected at 22.5° from the excitation beam. The slits were placed at 2.0 and 0.5 mm for excitation and emission, respectively, giving a bandwidth of 7.0 and 1.0 nm. Oriel 58916 (exc.) and Corning 97612 (em.) filters were used. Decay curves were measured with a SPEX 1934 phosphorimeter, Xe lamp (5 J/pulse).

The TG and DTA curves of the powders' thermal degradation after the heat treatment exhibited three stages of weight loss. The first stage of weight loss appeared between 80 and 250 °C and was caused by the evaporation of alcohol and desorption of the adsorbed moisture. The second stage occurred from 250 to 500 °C due to the pyrolysis of organic compounds, and the third stage occurred from 750 to 1,000 °C. This final weight loss was ascribed to the disappearance of residual alkoxy groups in the mineral matrix. In addition, the sharp exothermic peak located at 950 °C indicated crystallization of the gel [15, 16].

Results and discussion

XRD analysis

Figure 1 shows the XRD patterns of the YAG precursors sintered at 800 °C during various lengths of heat treatment time. The structure of the precursor powder of YAG:Eu prepared by the nonhydrolytic sol-gel process was examined by XRD. The XRD patterns revealed increased crystallization of the samples with longer heat-treatment times. The strongest peak appeared at $2\theta = 33.55°$ and corresponded to the lattice parameter [420], which is characteristic of the cubic system. In monoclinic systems, this peak occurs at $2\theta = 38.23°$. The diffraction pattern of the sample

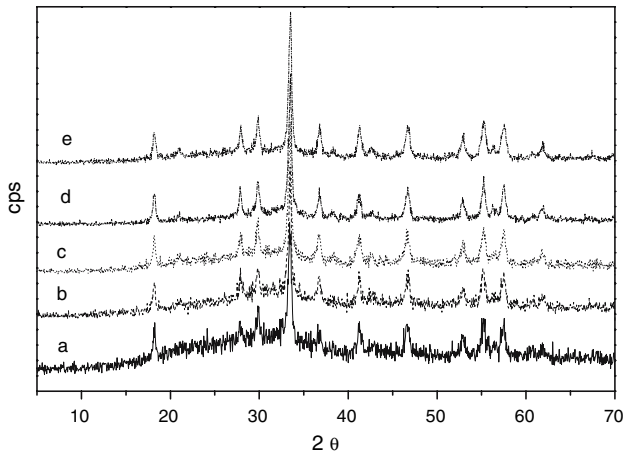

Fig. 1 XRD of samples treated at 800 °C for different lengths of time: (**a**) 1 h; (**b**) 2 h; (**c**) 4 h; (**d**) 8 h, and (**e**) 16 h

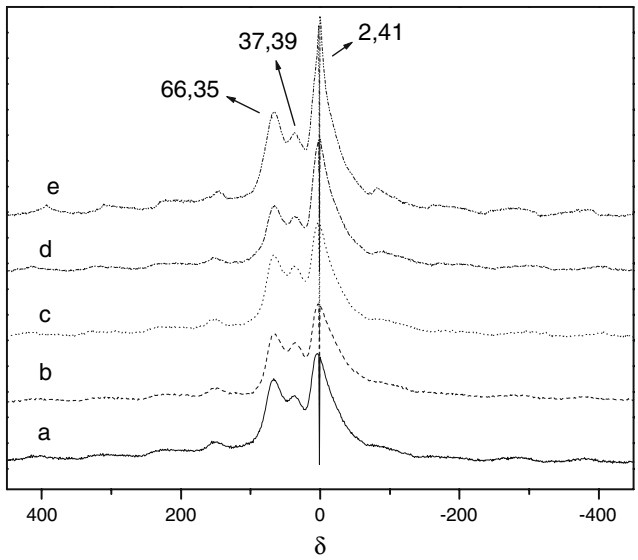

Fig. 2 ^{27}Al NMR spectra of the powder obtained at 800°C in different heat treatment times: (**a**) 1 h; (**b**) 2 h; (**c**) 4 h; (**d**) 8 h, and (**e**) 16 h

sintered at 800 °C indicated that all the peaks corresponded to the $Y_3Al_5O_{12}$ phase (JCPDS file 33–40). No other crystalline phase was detected. In conventional solid-state reactions [4] the YAG phase appears at 1,500 °C, and the literature reports on other procedures for preparing YAG using different methodologies and temperatures, e.g., 800 °C [15], 850 °C [17], 900 °C [18] and 1,000 °C [16].

Nuclear magnetic resonance ^{27}Al (NMR)

Figure 2 shows the spectra obtained for all the crystalline compounds. The NMR spectra of ^{27}Al calcined at different temperatures revealed the same behavior. We observed peaks at δ 2.41, 37.39 and 66.35 which correspond to six-(AlO_6), five-(AlO_5) and tetra-(AlO_4). The solid-state structure of $Y_3Al_5O_{12}$ consists of a network of 4- and 6-fold coordinated aluminum atoms. The yttrium atoms reside in the dodecahedral interstices formed by the corner-sharing arrangement of the AlO_4 and AlO_6 polyhedra [19]. Crystallographic data present a YAG cubic structure with 160 atoms per unit cell ($Z = 8$) with two AlO_6 and AlO_4 aluminum sites [20], confirming the crystallinity of compounds obtained by the nonhydrolytic sol-gel methodology.

Optical properties of YAG:Eu^{3+}

Figures 3 and 4 show the excitation spectra of Eu^{3+}-doped yttrium–aluminum oxide samples monitored at 591 nm ($^5D_0 \rightarrow {}^7F_1$) and 611 nm ($^5D_0 \rightarrow {}^7F_2$), respectively. The sharp lines were assigned to transitions from the $^7F_0$ level to $^5L_6$ (394 nm) and $^5D_{1-3}$ (405, 464 and 533 nm) levels in all the samples and are characteristic of the f ↔ f transition of the rare earth ion. The charge transfer (CT) band appeared in a region of high energy within a short wavelength of 200–300 nm. The CT band can show the degree of covalence of the Eu–Ligand bond, in which the shortest energy transition, the major interactions between metal and ligand [21]. Figure 3 depicts the CT band, which was probably located within a short wavelength, but the band shown in Fig. 4 was located at 258 nm in the sample treated for 1 h. Thereafter, the band shifted to a short wavelength, indicating that Eu^{3+}–O^{2-} had different covalences or different coordination sites.

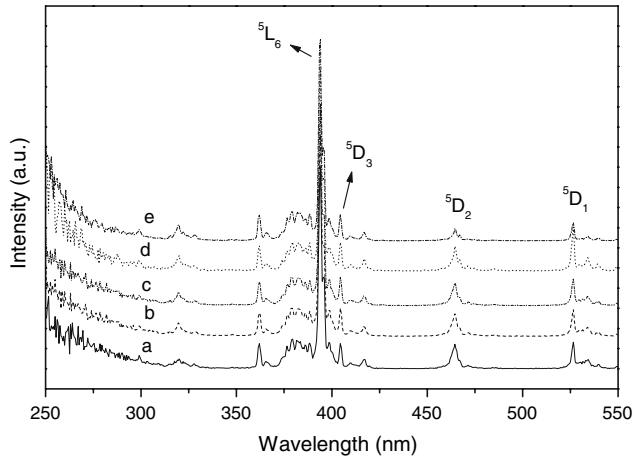

Fig. 3 Excitation spectra of the Eu^{3+} ion in Y–Al samples treated at 800 °C for different lengths of time: (**a**) 1 h; (**b**) 2 h; (**c**) 4 h; (**d**) 8 h, and (**e**) 16 h. Monitored at 591 nm ($^5D_0 \rightarrow {}^7F_1$)

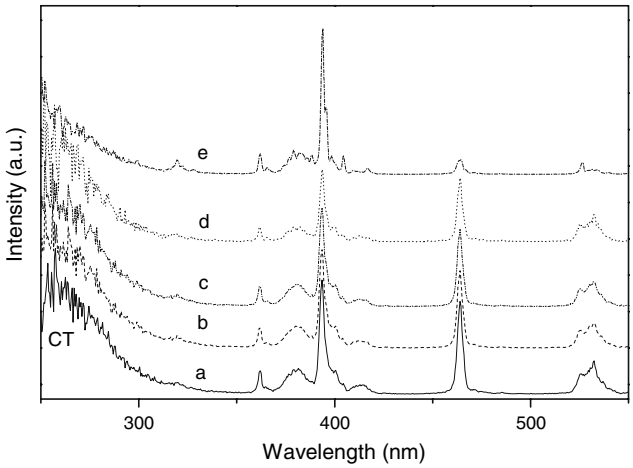

Fig. 4 Excitation spectra of the Eu^{3+} ion in Y–Al samples treated at 800 °C for different lengths of time: (**a**) 1 h; (**b**) 2 h; (**c**) 4 h; (**d**) 8 h, and (**e**) 16 h. Monitored at 611 nm ($^5D_0 \rightarrow {}^7F_2$)

The spectra illustrated in Fig. 3 are similar, but Fig. 4 shows that the intensity of the band corresponding to the $^5D_3$ transition (464 nm) decreased with rising temperature. The opposite type of transition occurred with $^5D_2$ (405 nm).

Figure 5 shows the emission spectra of Eu^{3+} ion recorded in the range of 550–720 nm for doped yttrium–aluminum oxide samples treated at 800 °C and excited at 394 nm ($^5L_6$ level). The emission spectra obtained by excitation in the $^5D_0 \rightarrow {}^5L_6$ transition of Eu^{3+} ion at 394 nm are composed of $^5D_0 \rightarrow {}^7F_J$ ($J = 0, 1, 2, 3$ and 4) emission lines of Eu^{3+}. The large magnitude of spin-orbit coupling in lanthanides causes the individual J levels of the various electronic terms to be well separated from one another, except for the

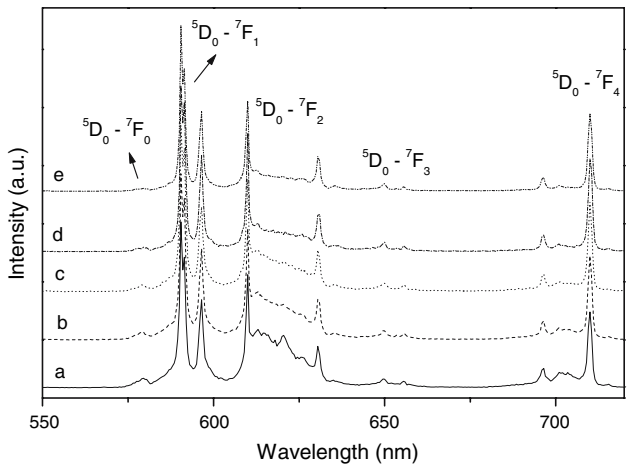

Fig. 5 Emission spectra of the Eu^{3+} ion in Y–Al samples treated at 800°C for different lengths of time: (**a**) 1 h; (**b**) 2 h; (**c**) 4 h; (**d**) 8 h, and (**e**) 16 h. Excited in 394 nm ($^5L_6$)

ground $^7F_0$ and emissive $^5D_0$ states of Eu^{3+}, which are nondegenerated. The highly forbidden $^7F_0 \rightarrow {}^5D_0$ transition of Eu^{3+} is particularly important in that only a single transition is possible for a single Eu^{3+} ion environment [22]. Figure 5 shows the $^7F_0 \rightarrow {}^5D_0$ transition in the samples treated for 1 h, revealing a decreased intensity, probably in response to a change in symmetry. The various J levels were further split by ligand fields in the maximum of $2J + 1$; therefore, in the $^7F_0 \rightarrow {}^5D_1$ and $^7F_0 \rightarrow {}^5D_2$ transition, the band numbers may be 3 and 5, respectively.

By applying the section rules for electric dipole (ED) and magnetic dipole (MD) transitions, the numbers of lines depend on the Eu^{3+} symmetry site, which can be determined by the allowed transitions [16]. It is well known that ED transitions are forbidden, since this type of transition only connects states of different parity. However, depending on the symmetry, interactions with the crystal field can alter the parity of the state. When the Eu^{3+} is located at a center of inversion, the $^5D_0 \rightarrow {}^7F_2$ emission should be suppressed and only the $^5D_0 \rightarrow {}^7F_1$ emission should occur [23]. The $^5D_0 \rightarrow {}^7F_1$ transition around 590 nm (MD) is more intense than $^5D_0 \rightarrow {}^7F_2$ (ED) transition, indicating that the Eu^{3+} ion is found in a symmetrical site with an inversion center. The ratio of the $^5D_0 \rightarrow {}^7F_2/{}^5D_0 \rightarrow {}^7F_1$ and $^5D_0 \rightarrow {}^7F_0/{}^5D_0 \rightarrow {}^7F_1$ emission decreased with longer heat treatment times, indicating increased symmetry of the crystal field.

Our X-rays showed the cubic phases of YAG. The literature [23] reports on two symmetrical sites: S_6 and C_2 to Eu^{3+} ion in yttrium oxide in this phase. The emission spectra shown here may indicate an increase in symmetry, probably from C_2 to S_6.

The experimental intensity parameters, Ω_2 and Ω_4, can be determined from the emission spectra of the Eu^{3+} ion based, respectively, on the $^5D_0 \rightarrow {}^7F_2$ and $^5D_0 \rightarrow {}^7F_4$ transitions [24–26]. Table 1 shows the spectroscopic intensity parameters, Ω_2 and Ω_4.

Table 1 Photoluminescence data of the YAG doped Eu^{3+} ion, heat-treated at 800 °C, in solid state

Samples (h)	Ω_2 (10^{-20} cm^2)	Ω_4 (10^{-20} cm^2)	τ (ms)	η (%)
1	0.94	4.11	2.48	28
2	1.15	4.29	2.31	28
4	1.23	4.31	2.42	30
8	1.51	4.40	2.40	32
16	1.64	5.61	2.81	45

Experimental intensity parameters Ω_2 and Ω_4, lifetimes (τ) and quantum efficiency (η), at room temperature

The values of the Ω_2 and Ω_4 parameters of the Eu^{3+}-doped YAG increased along with longer heat treatment times. Parra and Malta [24–26] observed high Ω_2 values (20 to 40×10^{-20} cm^2) in epoxy resin and rare earth complexes, reflecting the hypersensitive behavior of the $^5D_0 \rightarrow {}^7F_2$ transition. Lower Ω_2 values may indicate a weak chemical Eu–O polarization environment.

The emission quantum efficiency (η) of the ^5D_o to $^7F_2$ emission state was determined as described in Ref. [24]. As shown in Table 3, the values of lifetime and quantum efficiency for the samples heated for 1, 2, 4 and 8 h were similar. We observed an increase in the sample heated for 16 h, due to a better definition of the Eu^{3+} symmetry site.

Lifetime

Table 2 presents the lifetime of emissive $^5L_6$ and $^5D_2$ to ground $^7F_1$ and $^7F_2$ states for the samples treated for different lengths of heat treatment time.

We observed that the lifetime is independent of the heat treatment time. A long lifetime indicates a rigid system around the Eu^{3+} ion. The results in Table 4 reveal the dependence of the lifetime on the energy level. When the ion was excited at a level closer to the emission level ($^5D_0$), the lifetime was shorter. Depopulation of the $^5L_6 \rightarrow {}^5D_2$ level occurred rapidly (~0.4 ms), due to the closeness to the energy level.

Conclusions

The yttrium–aluminum system was synthesized by a nonhydrolytic sol-gel route through the condensation of aluminum chloride and ethanol with yttrium chloride in the presence of europium as structural probe.

The yttrium–aluminum materials thus obtained were heat-treated at 800 °C for 1, 2, 4, 8 and 16 h and then characterized by several techniques.

Table 2 Lifetime (τ (ms)) of the samples when excited at different levels: $^5L_6 \rightarrow {}^7F_2$ (394–611 nm), $^5D_2 \rightarrow {}^7F_2$ (464–611 nm), $^5L_6 \rightarrow {}^7F_1$ (394–590 nm) and $^5D_2 \rightarrow {}^7F_1$ (464–590 nm)

	1 h	2 h	4 h	8 h	16 h
394–611 nm	2.48	2.32	2.38	2.31	2.42
464–611 nm	1.99	1.90	1.98	1.91	1.94
394–590 nm	2.48	2.31	2.42	2.40	2.81
464–590 nm	2.09	2.00	2.07	2.01	2.12

The crystalline phase obtained after heat treatments at 800 °C for 16 h was characterized by X-ray diffraction as pure YAG yttrium–aluminum garnet. The ^{27}Al NMR spectra show evidence of sites characteristic of the YAG, confirming the formation of the crystalline YAG phase.

The lower values of the Ω_2 parameters of the Eu^{3+}-doped YAG possibly indicate a weak chemical Eu–O polarization environment.

YAG was successfully prepared by a nonhydrolytic sol-gel process at temperatures below those mentioned in the literature, which normally report obtaining this phase at temperatures exceeding 1,000 °C.

The material obtained in this study is potentially applicable in solid-state lasers and the lower temperature used in its preparation than by the conventional techniques offers energy savings and is environmentally friendly.

Acknowledgements The authors acknowledge FAPESP, CNPq and CAPES (Brazilian research funding agencies) for their financial support of this work.

References

1. Zhou YH, Lin J, Wang SB, Zhang HJ (2002) Opt Mater 20:13
2. Van der Weg WF, Robertson JM, Zwicker WK, Popma Th. JA (1989) J Lumin 24–25:633
3. Van der Weg WF, Popma Th. JA, Vink AT (1985) J Appl Phys 57:5450
4. Shi S, Wang J (2001) J Alloys Compd 327:82
5. Fernandez A, Somers J (2003) J Mater Sci 38:2331
6. Courrol LC, Zezell DM, Samad RE, Gomes L (2003) J Lumin 102–103:96
7. Wang HM, Simmonds MC, Huang YZ, Rodenburg JM (2003) Chem Mater 15:3473
8. Sardar DK, Yow RM, Gruber JB, Allik TH, Zandi B (2006) J Lumin 116:145
9. Ruan S-K, Zhou J-G, Zhong A-M, Duan J-F, Yang X-B, Su M-Z (1998) J. Alloys Compd 275–277:72
10. Weight JD, Sommerdijk NAJ (2003) In: Sol-Gel Materials Chemistry and Applications. Taylor & Francis Books
11. Apperley D, Hay JN, Raval HM (2002) Chem Mater 14:983
12. Hay JN, Raval HM (2001) Chem Mater 13:3396
13. Nassar EJ, Avila LR, Pereira PFS, Mello C, de Lima OJ, Ciuffi KJ, Carlos LD (2005) J Lumin 111:159
14. Acosta S, Corriu RJP, Leclercq D, Lefèvre P, Mutin PH, Vioux A (1994) J Non-Cryst Solids 170:234
15. Zhou YH, Lin J, Wang SB, Zhang HJ (2002) Opt Mater 20:13
16. Boyer D, Chadeyron GB, Mahiou R (2004) Opt Mater 26:101
17. Wang HM, Simmonds MC, Huang YZ, Rodenburg JM (2003) Chem Mater 15:3474
18. Towata A, Hwang HJ, Yasuoka M, Sando M, Niihara K (2002) Composites A 32:1127

19. Veith M, Mathur S, Kareiva A, Jilavi M, zimmer M, Huch V (1999) J Mater Chem 9:3069
20. Florian P, Gervais M, Douy A, Massiot D, Coutures J-P (2001) J Phys Chem B 105:379
21. Souza LA, Messaddeq Y, Ribeiro SJL, Fredericci C, Lanciotti F Jr, Pizani PS (2002) Quím Nova 25(6B):1067
22. de Horrocks W, Albin M Jr (1984) Prog Inorg Chem 31:1
23. Forest H, Ban G (1969) J Electrochem Soc Solid State Sci 116(4):474
24. Parra DF, Brito HF, Matos JD, Dias LC (2002) J Appl Polym Sci 83:2716
25. Malta OL, Brito HF, Menezes JFS, e Silva FRG, Alves Jr S, Farias FS Jr, de Andrade AVM (1997) J Lumin 75:255
26. Malta OL, Carlos LD (2003) Quim Nova 26(6):889